Numerical study on the influence of boundary conditions on the blast response of composite plates

To cite this article: L Lomazzi and A Vescovini 2022 *IOP Conf. Ser.: Mater. Sci. Eng.* **1214** 012005

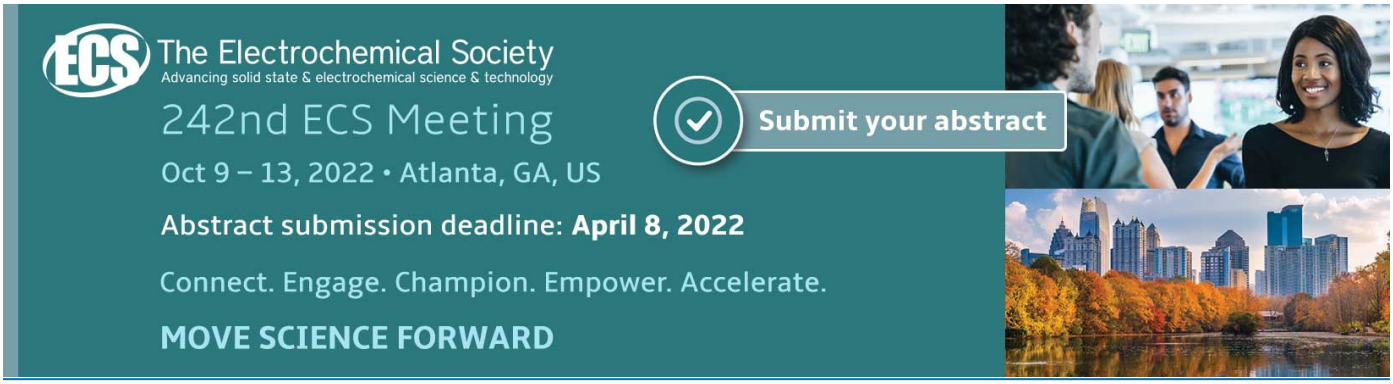

Numerical study on the influence of boundary conditions on the blast response of composite plates

L Lomazzi* and A Vescovini

Politecnico di Milano, Department of Mechanical Engineering, Via La Masa n.1, Milan, Italy

*Corresponding author: luca.lomazzi@polimi.it

Abstract. Blast loading represents a critical dynamic condition for both metal and composite structures. The blast response of metal materials has been extensively dealt with by researchers through experimental, analytical and numerical analyses, while composite materials appear to have been investigated in less detail. In this work, the blast response of a composite plate is numerically investigated employing the pure Lagrangian and the fully coupled Eulerian-Lagrangian (CEL) approaches using the LS-DYNA® software package. The latter methodology is set up to describe the effects determined by close-range explosions, such as the strongly non-uniform pressure distribution on the plate exposed area. Moreover, this work focuses on the characterisation of the influence of the boundary conditions on the plate response. The numerical methodology established in this work is set up and validated according to similar studies present in the literature.

1. Introduction

Composite structures are widely used in the structural engineering field and have several applications ranging from civil infrastructures, such as bridges and buildings, to mechanical systems, such as aircraft, ships and vehicles in general. Composite materials are also widespread in the military field, where they are commonly used both as part of high-performance protections, such as in protective panels for armoured vehicles, and for lightweight structures. Moreover, future trends in transportations are likely to move toward a larger use of this type of materials even for primary structures. Given the wide variety of applications, it is worth investigating the response of composite plate-like structures subjected to dynamic loading conditions, such as blast loading.

In the past fifty years many experimental tests have been performed to study the dynamic response of blast loaded plates with the purpose of formulating analytical and empirical predictive methods [1–5] or validating numerical models and methodological approaches [6–8]. The large number of studies published in the literature highlights that it is hard to accurately predict the dynamic response of plates subjected to blast loading, since it is determined by several multi-physics properties, such as the explosive material involved and its chemical composition and behaviour, the charge mass, the distance of the plate from the detonation point, the dimensions of the structure and the material it is made of.

Traditionally, most of the published works have only investigated the blast response of flat metallic monolithic plates. However, more recently, thanks to the increasing interest in advanced structural layouts and composite materials, experimental campaigns involving complex structures such as multi-layered plates [9] and structures made of composite materials [10–13] have been conducted. Similarly,

also analytical methods to predict the blast response of composite plate-like structures have been recently propounded in the literature [14–17]. However, so far, the available analytical theories can only deal with simple boundary conditions and geometries and do not consider complex physical phenomena, such as the extremely non-linear effects rising in case of failure of composite plates.

Hence, finite element (FE) techniques are usually employed to deal with complex structures subjected to dynamic loading from nearby explosions [17]. This type of numerical simulations can also take into account the non-linear post-failure behaviour of composite materials, that reveals to be paramount to satisfactorily reproduce the blast loaded plate response [12,18,19]. However, to date, a limited number of numerical models employed to simulate composite plates under blast loading have been validated with experimental observations [17]. An exception is represented by the works in [12,13], that present a validated FE model of carbon fibre-polymer laminates and of woven glass/epoxy composite plates subjected to blast loading, respectively. Moreover, almost all the works present in the literature characterise the blast wave-structure interaction using the pure Lagrangian approach, that is known not to be accurate enough in close-range scenarios [20] and cannot predict eventual fluid-structure interaction (FSI) effects [21].

In this work, two methodological approaches to simulate the blast wave propagation and interaction with the target structure, i.e, the pure Lagrangian approach and the fully coupled Eulerian-Lagrangian (CEL) approach, are presented and the potentialities of each method are investigated by means of a case study taken from the experimental campaign presented in the work in [12], that involves carbon fibre-polymer laminates under blast loading. Moreover, the influence of the technique employed to model the plate boundary conditions on the structural response is investigated. This work is organised as follows. Section 2 presents and discusses the methodological approaches employed in this work to simulate the dynamic response of blast loaded composite plates. Section 3 presents a case study to investigate the potentialities of the two approaches and to characterise the influence of the modelling technique adopted to simulate the plate boundary conditions on the structural response. Finally, Section 4 discusses the main results of the case study and Section 5 draws out the conclusions from this work.

2. Methodological approach

Two approaches to the numerical simulation of blast loaded structures are investigated in this work, i.e., the pure Lagrangian approach and the fully coupled Eulerian-Lagrangian technique.

In this Section, the two approaches mentioned above are briefly described, along with the methodology set up to model the target structure. No mention to the specific solver used in this work is made in this Section, since all the information about the case study and the modelling procedure involved are reported in detail in Section 3.

2.1. Pure Lagrangian approach

A pure Lagrangian analysis consists of modelling the structure with Lagrangian elements and predicting the blast pressure time history exploiting empirical equations. The blast pressure is exerted on the structure as an analytical pressure load resorting to the specific equations implemented in the software package employed for the analysis. In particular, in this work the Kingery-Bulmash equations are exploited to predict the blast loading properties due to the explosion of some high explosive (HE) material [22]. Such equations, which were obtained via model fitting to experimental results, only require as input value the scaled distance *Z*, which is defined according to Equation 1 [23,24]:

$$Z=\frac{R}{W_{TNT}^{1/3}}\ (1) \tag{1}$$

where *R* is the standoff distance, i.e., the distance from the centre of the HE spherical charge to a specific point of interest, while W_{TNT} is the TNT equivalent weight of the explosive material considered. The Kingery-Bulmash relationships employed in this work are valid at scaled distance

values 0.147 m/kg$^{1/3}$<Z<40 m/kg$^{1/3}$, below this limit the predicted blast parameters may be inaccurate [25].

Instead, the analytical pressure applied to the target structure is typically computed according to Equation 2 [26]:

$$P = P_R \cdot \cos^2\theta + P_I \cdot (1 + \cos^2\theta - 2 \cdot \cos\theta) \quad (2)$$

where P_R and P_I are the reflected and the incident pressure values estimated by the Kingery-Bulmash equations, respectively, while θ is the angle of incidence. Note that Equation 2 is not valid for negative values of cosθ, i.e., for points on the surface not facing the explosion. In such a case, the simplified relationship $P=P_I$ is considered. The value of P is computed at each iteration of the solution for each loaded element, since (i) the variable θ varies during the structural deformation process and (ii) the values of P_R and P_I depend both on the spatial position of the target element with respect to the detonation point and on the time passed from the detonation of the HE material. No more information is reported in this work on the analytical prediction of blast loading. The interested reader is referred to the work in [27] to go deeper into the topic and for a critical discussion of Equation 2.

The blast loading prediction in the pure Lagrangian approach is not a computationally critical operation, since only empirical and analytical equations are involved, but no fluid structure interaction effects can be evaluated using this method, i.e., the effect of the deformation rate of the structure on the pressure loading is neglected.

2.2. Fully coupled Eulerian-Lagrangian approach

A CEL analysis consists of modelling both the target structure, exploiting the Lagrangian elements formulation, and the HE charge and the surrounding material, resorting to the Eulerian elements formulation. The thermodynamic state evolution of the HE material after the detonation event is determined employing the Jones-Wilkins-Lee (JWL) equation of state shown in Equation 3 [28]:

$$P(V,e) = A\left[1 - \frac{\omega \cdot V_0}{V \cdot R_1}\right] \cdot e^{-\frac{V \cdot R_1}{V_0}} + B\left[1 - \frac{\omega \cdot V_0}{V \cdot R_2}\right] \cdot e^{-\frac{V \cdot R_2}{V_0}} + \omega \rho e \quad (3)$$

where V is the inverse of density ρ, *e* the internal energy, A and B parameters with the units of pressure, ω the Grüneisen coefficient and R_1 and R_2 dimensionless parameters. The shock wave produced by the detonation of the explosive charge propagates in the surrounding material and reaches the target structure exerting on it a pressure loading. Hence, the surrounding material, i.e., the air in this work, needs to be modelled as well. In particular, the ideal gas equation of state shown in Equation 4 is typically assigned to the air domain [29]:

$$P = \rho \cdot (C_p - C_v) \cdot T \quad (4)$$

where C_p and C_v are the specific heat at constant pressure and at constant volume, respectively, while T is the temperature.

The thermodynamic state evolution of the HE material, the shock wave development and propagation in air and the prediction of the pressure load exerted on the structure are computationally expensive operations and usually represent the bottleneck of the CEL approach. Despite this issue, complex phenomena such as fluid structure interaction effects can be evaluated employing the fully coupled Eulerian-Lagrangian approach.

In this work, a hybrid modelling technique is presented that makes the CEL approach less computationally expensive. In particular, the explosive charge is not explicitly modelled, but only the air domain surrounding the target structure is considered. The shock wave is introduced in the simulation by loading the air domain with an analytical pressure time history determined resorting to

the Kingery-Bulmash equations referred to in Section 2.1. This technique allows analytically propagating the blast wave to a region close to the target structure, saving the time required to numerically simulate the HE material detonation and the formation and propagation of the shock wave far from the region of interest. The proposed CEL methodology is shown in Figure *1*. Note that this hybrid technique may inaccurately characterise the blast loading if the scaled distance value Z evaluated considering as standoff distance R the distance R_{EUL} (Figure *1*) from the detonation point to the closest air domain point, i.e., $Z_{EUL}=R_{EUL}/W_{TNT}^{1/3}$, does not meet the requirement $0.147\ m/kg^{1/3}<Z_{EUL}<40\ m/kg^{1/3}$.

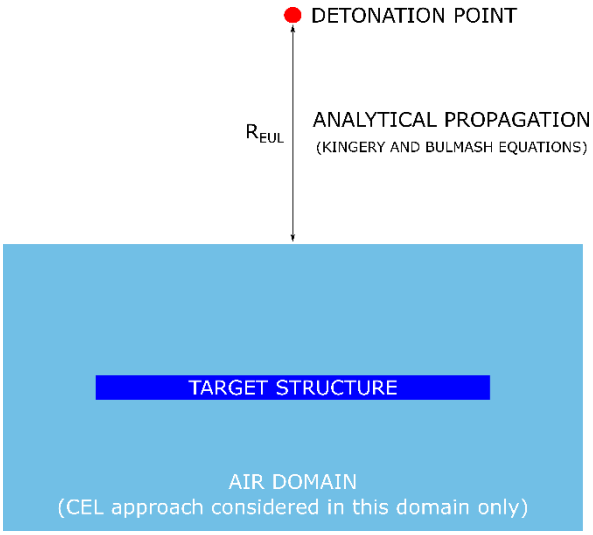

Figure 1. Proposed solution to speed up the CEL approach.

2.3. Target structure modelling approach

The target structure is modelled exploiting the Lagrangian elements formulation. Solid elements are preferred to shell elements in this work. This choice is made since the authors verified that the fully coupled Eulerian-Lagrangian approach works better with structures modelled as solid entities, even though shell elements would speed up the computations. The simulations proving this statement are not reported here for the sake of brevity. The composite material is modelled with a macro-homogeneous discretisation, i.e., each ply is modelled with a layer of solid elements. The intra-laminar and inter-laminar properties of the composite material are both retained in the analyses. The former is assigned to the solid elements representing each ply, while the latter is implemented as contact interaction between adjacent layers. More information about the specific properties of the structural elements is reported in the next Section with reference to the case study.

3. Case Study

The methodological approaches described in Section 2 are herein employed to simulate one of the experimental scenarios presented in the work in [12]. In this Section, the case study setup is briefly introduced and the numerical simulations are described in terms of main modelling parameters and results. Moreover, within the subsection dedicated to the CEL analysis, the influence of the modelling technique employed to apply the boundary conditions of the blast loaded structure is investigated. All the numerical simulations are performed employing the LS-DYNA® software package.

3.1. Description of the scenario under assessment

The scenario considered in this work involves the detonation of a 100g spherical Type 4 plastic explosive charge at 0.4m standoff distance from a flat quadrangular plate. The blast loaded plate is a Carbon-Polyester laminate composed of seven plies with thickness 0.6mm each and has dimensions

275x275mm^2. Each ply is made of plain-woven fabric. The plate is fixed to a support structure by means of a steel window frame leaving an exposed area of 250x250mm^2. Soft EPDM 414 foam is placed between the steel frame and the plate to create a simply supported-like boundary condition for the blast loaded structure. The scenario considered in this case study is shown in Figure *2*.

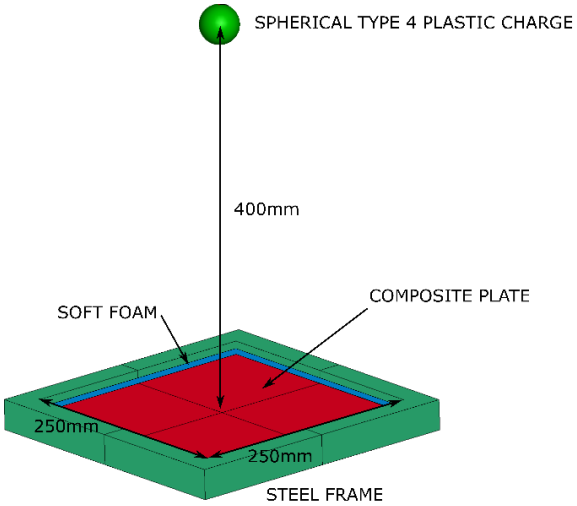

Figure 2. Scenario considered in the case study.

Note that the scenario described above is taken from the work in [12], where the experimental campaign is presented along with the numerical simulation performed employing the pure Lagrangian approach in the Abaqus® software package.

3.2. Modelling of the structural elements

In this subsection the modelling technique and parameters employed to model the steel window frame, the foam and the composite plate are presented.

The steel window frame is modelled using solid hexahedral elements with characteristic dimension 2.45mm and fully integrated formulation (elform=-1). Steel is modelled resorting to the elastic isotropic constitutive law implemented in LS-DYNA® with MAT_001 (*MAT_ELASTIC) using the parameters shown in Table 1, where RO identifies the material density, E the elastic modulus and PR the Poisson ratio.

Table 1. Parameters of the material of the steel frame [12].

Steel - MAT_001	
RO	7800 kg·m^{-3}
E	203 GPa
PR	0.3

The foam placed between the steel clamp and the composite plate is the soft EPDM 414 foam. However, in the work in [12] the material parameters employed in the constitutive law are not reported. Hence, since to the authors' best knowledge no information is present in the literature about the specific foam employed in the experimental setup, a different foam taken from the work in [30] is modelled in this case study. This choice is not considered to be critical for the numerical simulations since the foam is only employed to simulate simply supported-like boundary conditions and the stress state of this component is not investigated. Solid hexahedral elements with characteristic dimension 2.5mm are employed to model the foam material. Since this component is expected to undergo large

deformations, a reduced integration element formulation (elform=1) is chosen to avoid possible negative volume errors preventing the normal termination of the numerical simulations. Moreover, to the same purpose, erosion is added to the material constitutive law to delete excessively distorted elements using the material card MAT_000 (*MAT_ADD_EROSION), setting the maximum effective strain at failure EFFEPS value to 5. The material constitutive law is implemented resorting to the LS-DYNA keyword MAT_057 (*MAT_LOW_DENSITY_FOAM), that is a law dedicated to highly compressible low density foams. The main material parameters are shown in Table *2*, where E identifies the Young's modulus used in tension, LCID the ID of the curve of the nominal stress versus strain, HU the hysteretic unloading factor, BETA the decay constant to model creep in unloading, DAMP the viscous coefficient to model damping effects, SHAPE the shape factor for unloading and KCON the stiffness coefficient for contact interface stiffness. The fields left to the default value are not shown in Table *2*, the interested reader is referred to the LS-DYNA® keyword user's manual (Vol. II) to go deeper into the topic [29].

Table 2. Parameters of the material of the foam [30,31].

Foam - MAT_057	
RO	63 kg·m^{-3}
E	8.4 MPa
LCID	Curve taken from [30]
HU	0.25
BETA	5.0
DAMP	0.5
SHAPE	5.0
KCON	1150 MPa

Each ply of the composite plate is modelled with solid hexahedral elements with characteristic dimension 2mm, as suggested in the work in [12], using one element in the thickness. A fully integrated element formulation (elform=-1) is employed to avoid hourglass effects. The intra-laminar properties are defined describing the composite material constitutive law employing the LS-DYNA® keyword MAT_054 (*MAT_ENHANCED_COMPOSITE_DAMAGE), that represents a built-in material model based on the Hashin failure criteria [32]. The main non-default material properties considered in this work are reported in Table 3, where EA, EB and EC are the Young's moduli in the three principal directions, PRBA is the in-plane Poisson ratio and GAB, GBC and GCA are the shear moduli in the three principal planes. Moreover, the parameter 2WAY=1 represents a flag to turn on the 2-way fibre action, DFAILT and DFAILC are the maximum strain values for fibre tension and compression, respectively, that are intentionally set to large values to avoid element deletion and to replicate the same conditions considered in the work in [12]. Finally, XC, XT, YC and YT are the strength values for the in-plane compressive (C) and tensile (T) modes and SC is the shear strength, that is intentionally set to a large value to neglect its contribution to the material failure [12].

Table 3. Material properties of the Carbon-Polyester laminate plies [12].

Carbon-Polyester laminate ply - MAT_054	
RO	1600 kg·m^{-3}
EA	55 GPa
EB	55 GPa
EC	7 GPa
PRBA	0.25
GAB	4.5 GPa
GBC	1.8 GPa

GCA	1.8 GPa
2WAY	1
DFAILT	1
DFAILC	-1
XC	240 MPa
XT	680 MPa
YC	240 MPa
YT	680 MPa
SC	1000 MPa

The inter-laminar properties are modelled employing the Cohesive Zone Model (CZM) approach using the keyword *CONTACT_AUTOMATIC_SURFACE_TO_SURFACE_TIEBREAK. This contact algorithm keeps the corresponding nodes between adjacent layers connected until failure occurs; after that, the interaction is turned into a simple surface-to-surface contact between the plies. Failure is accounted for by means of a quadratic criterion that considers both the normal and the shear interlaminar stresses. The maximum normal (NFLS) and shear (SFLS) stress values considered in this work are reported in Table 4.

Table 4. Properties of the contact interaction between adjacent plies [12].

NFLS	60 MPa
SFLS	60 MPa

The finite element model of the structural components is shown in Figure *3*, where the reference system considered in the analysis is also presented. The plate surface facing the blast loading lies in the xy plane characterised by z=0m and the plate central point on the same surface is at coordinates x=y=0m. Note that only a quarter of the model is considered to speed up the computations, accordingly introducing symmetry constraints on the x and y negative faces.

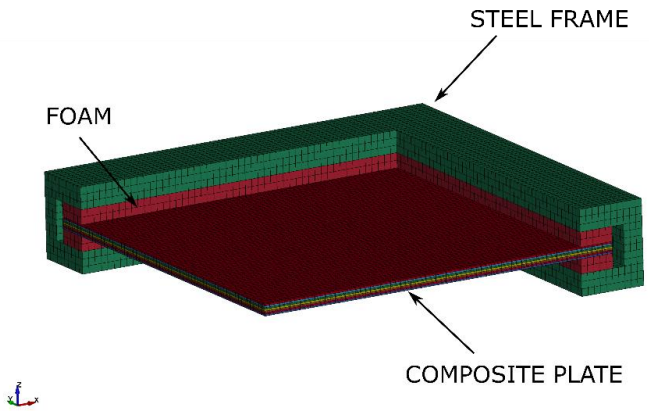

Figure 3. Finite element model of the structural components.

Contact algorithms are employed to consider in the numerical simulations the eventual interaction between the structural components. The foam is glued to the steel frame to reproduce the foam lined frame configuration referred to in the work in [12]. This is achieved introducing in the numerical analysis the keyword *CONTACT_TIED_SURFACE_TO_SURFACE with pinball segment based contact (SOFT=2) option. The contact between the foam and the plate is described using the algorithm *CONTACT_ERODING_SURFACE_TO_SURFACE with pinball segment based contact (SOFT=2) option and static and dynamic coefficients of friction FS=1 and FD=1, respectively [33,34]. This

contact algorithm allows tracking the contact between the involved parts even if they undergo erosion, as it might happen to the foam elements as discussed above.

Boundary conditions are introduced to reproduce the effect of the experimental support structure. Two different models are set up to evaluate the effect of the modelling of the boundary conditions on the blast loaded plate response. The first model is hereinafter referred to as *CBC* (Complete Boundary Conditions) model, it consists of the whole setup shown in Figure *3* to which an encastre boundary condition is applied on the steel frame face opposite to the explosive charge. Instead, the second model, which is hereinafter referred to as *SBC* (Simplified Boundary Conditions) model, only includes the plate exposed area and the encastre boundary condition is applied to the edges of the plate. The two models are compared in Figure *4*.

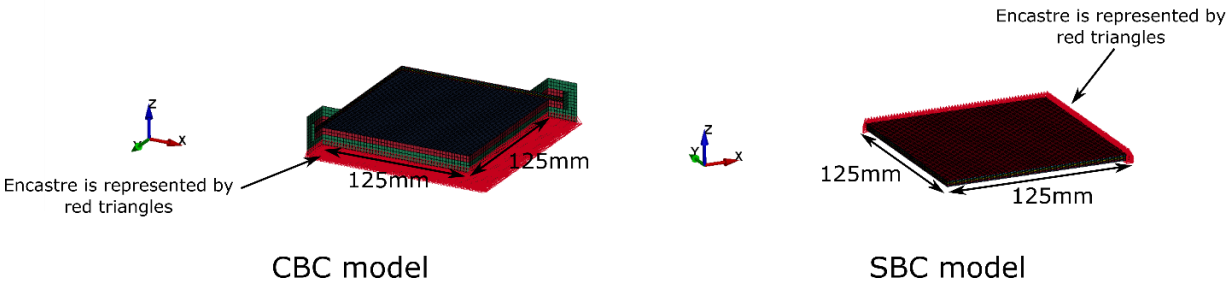

Figure 4. Boundary conditions modelling strategies.

3.3. Pure Lagrangian analysis

In the pure Lagrangian analysis the blast loading is applied on the plate exposed area facing the explosive charge according to the approach described in Section 2.1. The blast pressure loading is determined employing the keyword *LOAD_BLAST_ENHANCED with the parameters shown in Table *5*, where M is the TNT equivalent weight of the explosive material (referred to as W_{TNT} in Section 2.1), XBO, YBO and ZBO the coordinates of the explosive charge in the reference system shown in Figure *4*, TBO the time of detonation, BLAST=2 the flag to specify that the explosion is a spherical free-air burst and NEGPHS=0 the flag to retain the blast pressure negative phase in the analysis.

Table 5. Parameters to compute the blast loading in the pure Lagrangian approach.

*LOAD_BLAST_ENHANCED	
M	168 g
XBO	0 m
YBO	0 m
ZBO	0.4 m
TBO	-0.13 ms
BLAST	2
NEGPHS	0

Looking at the data reported in Table *5*, the explosive charge is placed at a standoff distance of 0.4m from the plate surface facing the blast load and the equivalent TNT weight of the 100g spherical Type 4 plastic explosive charge is M=168g. This TNT equivalent weight value is determined employing the equations proposed in [35] that satisfy the equivalence in terms of blast pressure prediction. In particular, to stay on the conservative side, the upper bound value of the TNT equivalent weight is adopted in this work. According to the standoff distance and the TNT weight considered in the analysis, the scaled distance value associated to the explosion is Z=0.72 m/kg$^{1/3}$, which satisfies the requirement for the validity of the Kingery-Bulmash equations reported in Section 2.1. Note that, to reduce the computational time, the arrival time (AT) of the blast wave is estimated using the Kingery-Bulmash equations and the analysis is started right before the wave impacts the structure. This is achieved by specifying a negative value in the field TBO so that |TBO|<AT.

The blast pressure and impulse exerted on the centre of the plate are shown in Figure *5*.

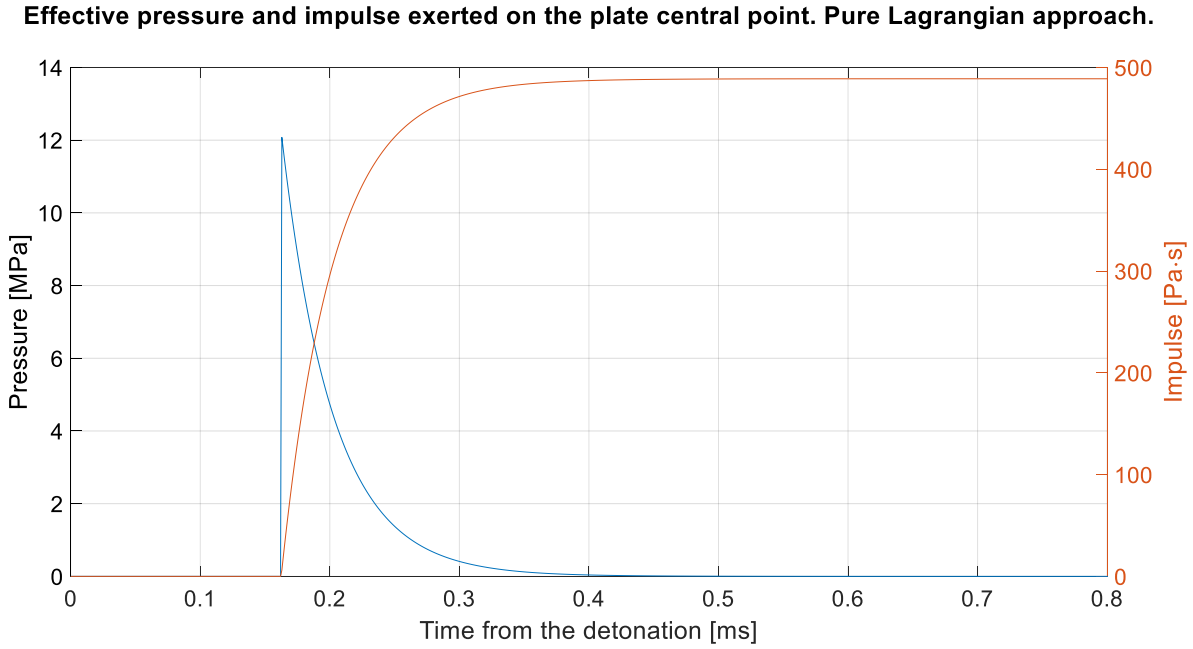

Figure 5. Effective pressure and impulse exerted on the plate central point. Pure Lagrangian approach.

The absolute value of the displacement of the plate centre is shown in Figure *6* for the only *CBC* model, since the *SBC* model is not assessed using the pure Lagrangian approach. Note that the absolute value of the displacement is plotted since, usually, positive values are shown in the literature, while according to the reference system shown in Figure *4* the plate gets deformed in the negative z direction in this case study.

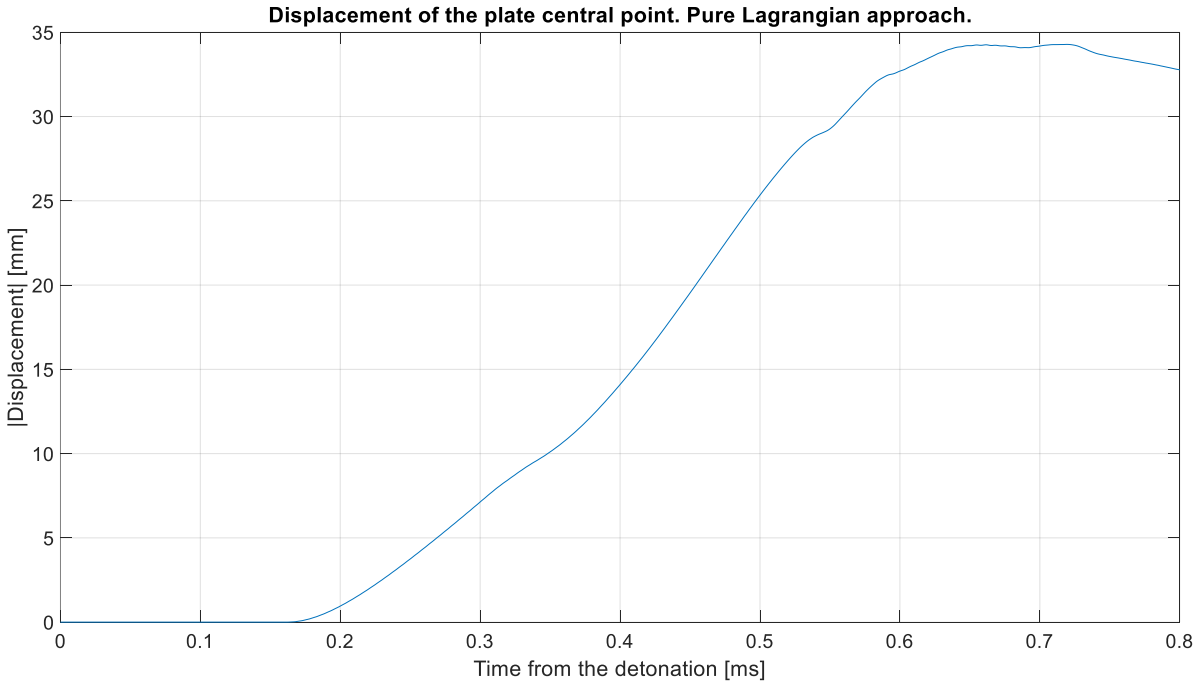

Figure 6. Absolute value of the displacement of the plate central point. Pure Lagrangian approach.

A summary of the maximum registered pressure (p_{max}^{Lag}), impulse (i_{max}^{Lag}) and displacement ($d_{max}^{Lag,\ CBC}$) at the central point of the plate is reported in Table *6*. The apex *Lag* identifies the results from the pure Lagrangian analysis, the apex *CBC* identifies the *CBC* model.

Table 6. Summary of the pure Lagrangian analysis results.

p_{max}^{Lag}	12.1 MPa
i_{max}^{Lag}	488.9 Pa·s
$d_{max}^{Lag,CBC}$	34.3 mm

3.4. CEL analysis

According to the CEL approach introduced in Section 2.2, the blast wave propagation and its interaction with the target structure are dealt with by explicitly modelling the air domain exploiting solid hexahedral elements with characteristic dimension at convergence 1mm. The formulation selected in this work is the solid section elform=5, which identifies 1 point Arbitrary Lagrangian-Eulerian (ALE) elements. The keyword *ALE_REFERENCE_SYSTEM_GROUP is employed to model the behaviour of the ALE elements. In particular, the air domain is assigned a mesh smoothing option dedicated to scenarios involving shock waves (PRTYPE=8) and the pure Eulerian behaviour is forced setting the initial mesh remapping factor (EFAC) to 1. Moreover, the card *CONTROL_ALE is included in the analysis to set the following global control parameters for the Eulerian calculations. The advection method employed in the analysis is the *donor cell + HIS* method (METH=3), which is a first order accurate method conserving total energy over each advection step. The ALE mesh smoothing is turned off (AFAC=-1) and flow out boundary conditions are specified at the Eulerian boundaries to avoid undesired reflections of the shock wave as it impacts the mesh boundary (EBC=0). Finally, the reference pressure value applied to the free surfaces of the ALE mesh boundary (PREF field) is set to 101,325 Pa. The CEL model is shown in Figure *7*.

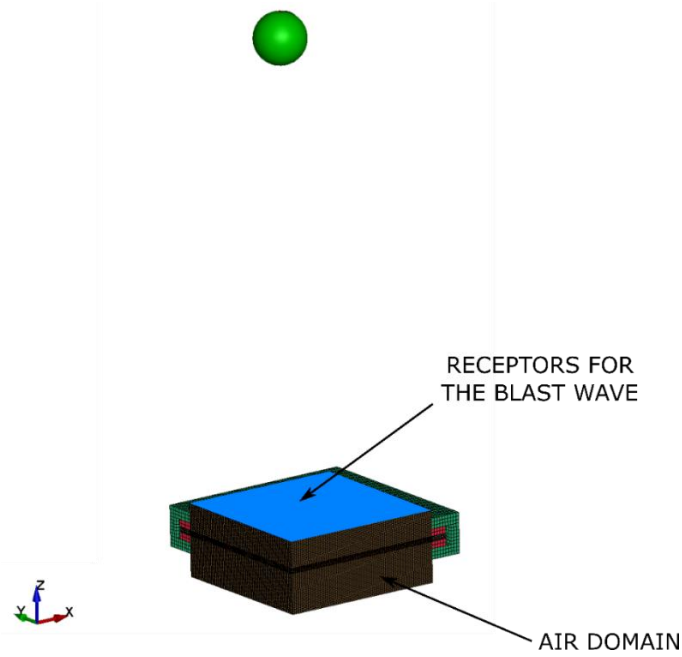

Figure 7. Finite element model involved in the CEL analysis.

The air behaviour is modelled using the material model MAT_009 (card *MAT_NULL) and the ideal gas equation of state (card *EOS_IDEAL_GAS). The non-default parameters included in the analysis are reported in Table *7*, where MU identifies the dynamic viscosity, CV0 and CP0 the specific heat constants for the definition of C_v and C_p, respectively, V0 the initial relative volume and T0 the initial temperature value.

Table 7. Parameters to model the air behaviour [36,37].

Air - MAT_009	
RHO	1.225 kg·m^{-3}
MU	1.8·10^{-5} Pa·s
Air - *EOS_IDEAL_GAS	
CV0	717 J·Kg^{-1}·K^{-1}
CP0	1007 J·Kg^{-1}·K^{-1}
V0	1
T0	288.15 K

According to the procedure described in Section 2.2, the shock wave is initiated in the air domain by loading its upper surface with the analytical prediction from the Kingery-Bulmash equations. The elements acting as receptors for the blast wave are included into a segment set (see Figure *7*) that is specified in the card *LOAD_BLAST_SEGMENT_SET. In this card, the field SFNRB is set to 1 to attenuate the shock waves reflected back to the ambient elements. The parameters included in the *LOAD_BLAST_ENHANCED card to define the blast load are the same as the parameters shown in Table *5*. According to the standoff distance (R_{EUL}=380mm) and the TNT weight considered in the analysis, the scaled distance value associated to the explosion is Z=0.69 m/kg$^{1/3}$, which satisfies the requirement for the validity of the Kingery-Bulmash equations reported in Section 2.1.

Symmetry boundary conditions are applied to the x and y negative surfaces of the Eulerian domain, as also described in Section 3.2 for the structural components. The interaction between the shock wave propagating in the air domain and the composite plate is set up employing the card *CONSTRAINED_LAGRANGE_IN_SOLID. In this card, the air domain is set as master part, while

the set of plies is specified in the slave field. Moreover, the fluid-structure coupling method CTYPE=4 is considered in the analysis, which is a penalty coupling for solid elements without erosion.

The blast pressure and impulse exerted on the centre of the plate are shown in Figure *8*.

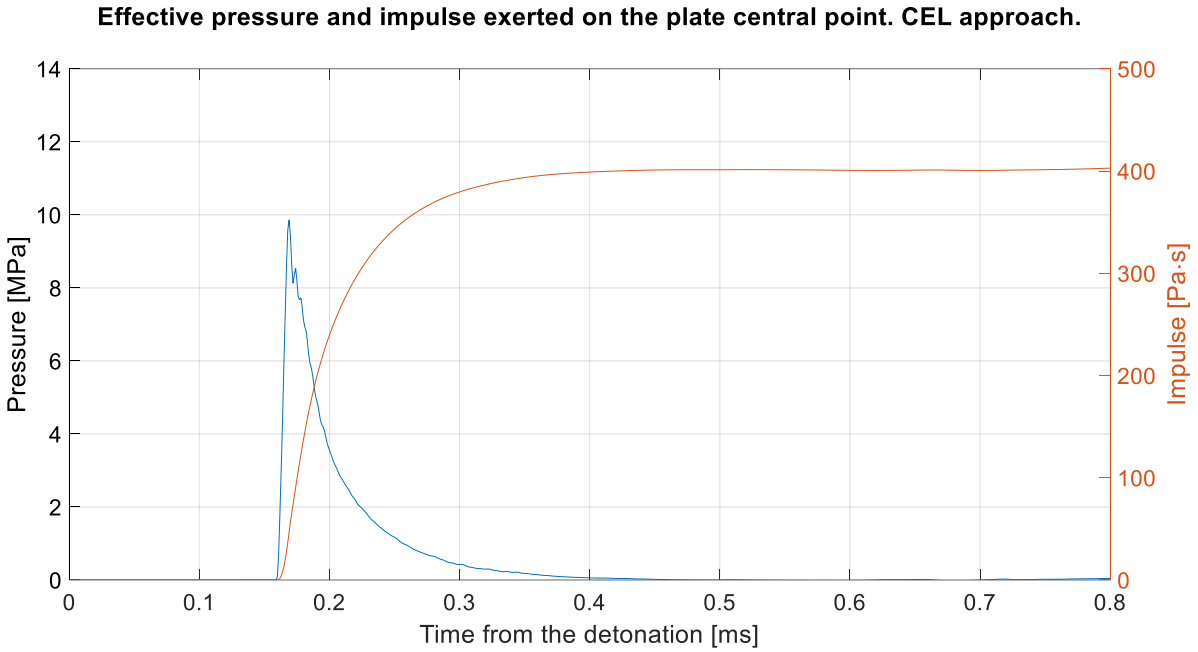

Figure 8. Effective pressure and impulse exerted on the plate central point. CEL approach.

The absolute value of the displacement of the plate centre is shown in Figure *9* for the *CBC* model (solid curve) and for the *SBC* model (dashed curve). The curve obtained with the *SBC* model is stopped as soon as the plate passes through the initial position.

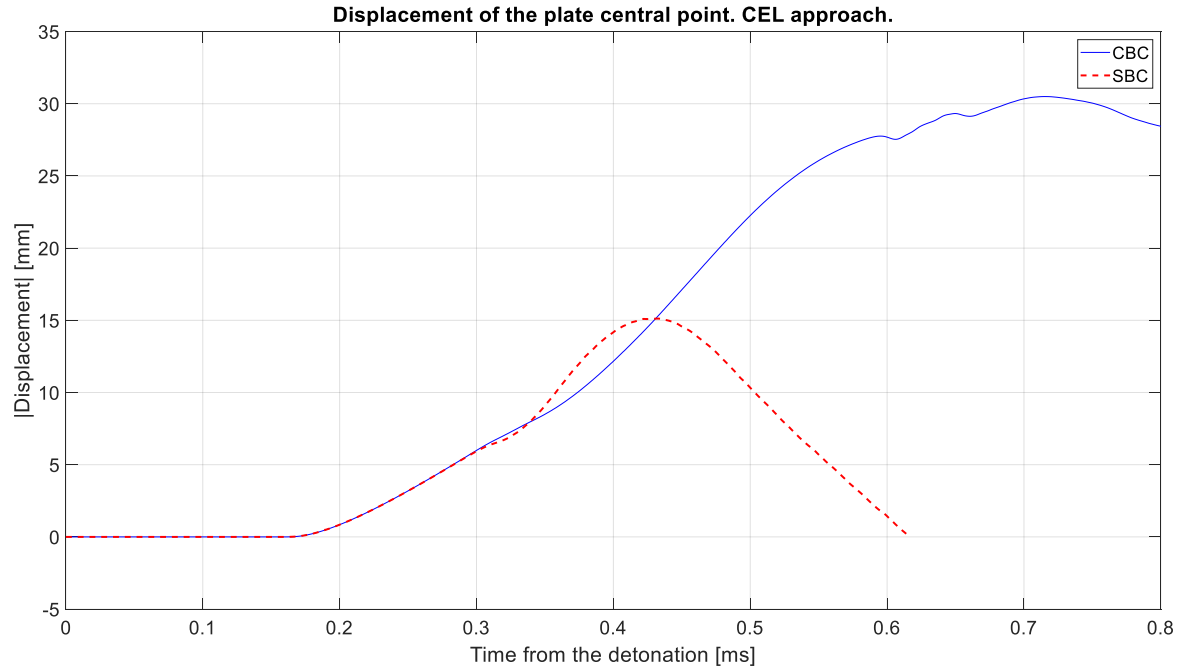

Figure 9. Absolute value of the displacement of the plate central point. CEL approach.

A summary of the maximum registered pressure (p_{max}^{CEL}), impulse (i_{max}^{CEL}) and displacement (d_{max}^{CEL}) at the central point of the plate is reported in Table *8*. The apex *CEL* identifies the results from the CEL analysis, the apex *SBC* identifies the *SBC* model.

Table 8. Summary of the CEL analyses results.

p_{max}^{CEL}	10.0 MPa
i_{max}^{CEL}	405.3 Pa·s
$d_{max}^{CEL,CBC}$	30.5 mm
$d_{max}^{CEL,SBC}$	15.1 mm

4. Discussion

In this Section, the results of the numerical simulations presented in Section 3 are discussed and compared.

The deflection time histories of the plate centre predicted by the numerical analyses presented in this work are shown in Figure *10*, along with the experimentally measured maximum displacement.

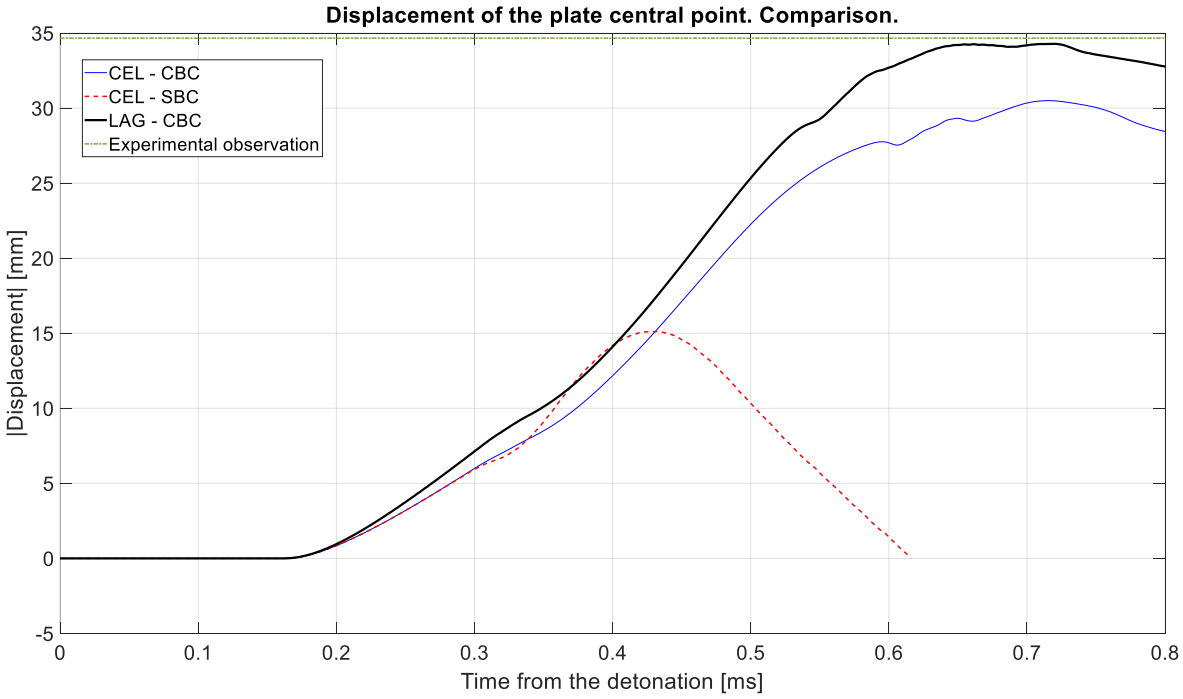

Figure 10. Displacement of the plate central point.

It turns out that the model with simplified boundary conditions (SBC) underestimates the deflection time history of the plate centre, while the CBC models satisfactorily reproduce the experimental observation. To further prove this, the maximum displacement values are compared in Table *9* considering the numerical models ($d_{max}^{Lag,CBC}$, $d_{max}^{CEL,CBC}$, $d_{max}^{CEL,SBC}$) and the experimental observation (d_{max}^{Exp}). The error affecting the *ith* numerical prediction is computed according to Equation 5, where the apex *i* identifies the numerical analysis of interest, i.e., *i* can assume the values *Lag,CBC*, *CEL,CBC* and *CEL,SBC*.

$$\text{Error}^{i}=\frac{d_{max}^{i}-d_{max}^{Exp}}{d_{max}^{Exp}}\cdot 100\% \quad (5)$$

Table 9. Comparison of the maximum deflection of the plate centre.

		Error
d_{max}^{Exp}	34.7 mm [12]	~
$d_{max}^{Lag,CBC}$	34.3 mm	-1.2%
$d_{max}^{CEL,CBC}$	30.5 mm	-12.1%
$d_{max}^{CEL,SBC}$	15.1 mm	-56.5%

The results shown in Table *9* confirm that the CBC models satisfactorily reproduce the experimentally observed maximum deflection of the plate centre, while the SBC setup strongly underestimates this value. This result suggests that accurately modelling the boundary conditions of the blast loaded structure is paramount to satisfactorily reproduce the real scenario.

Moreover, the Lagrangian analysis seems to provide more accurate results than the fully coupled Eulerian-Lagrangian approach. This result needs a deeper investigation to be explained, since the work in [12] labels the scenario assessed in the case study as near-field explosion (or close-range explosion), which usually requires the CEL approach for an accurate characterisation of the underlying physical phenomena involved. The near-field or far-field nature of an explosive scenario is determined by the value of the radial expansion of the shock front at the plate location ($\bar{r}_{plate}$), that is computed according to Equation 6:

$$\bar{r}_{plate}=\frac{\text{standoff distance}}{\text{charge radius}} \quad (6)$$

Typically, close-range effects are relevant for $1<\bar{r}_{plate}\leq 10$, while far-field conditions can be safely assumed for explosions characterised by $\bar{r}_{plate}>10$ [38]. The former case requires employing fully coupled Eulerian-Lagrangian analysis to satisfactorily reproduce the experimental observations, while the latter can be safely simulated employing the pure Lagrangian approach [20]. In the case study presented in this work, considering the explosive charge as a sphere of TNT with density 1610 $kg \cdot m^{-3}$ [39], the radial expansion of the shock front at the plate location value is $\bar{r}_{plate}=13.7$, that identifies a far-field scenario. Hence, the pure Lagrangian approach is suitable to simulate the explosive event and no improvement is expected by performing the CEL analysis. The smaller maximum deflection of the plate centre predicted using the fully coupled approach is determined by the lower peak effective pressure and impulse imparted to the blast loaded structure than the values determined by the pure Lagrangian approach, as shown in Figure *11* and Figure *12*, respectively.

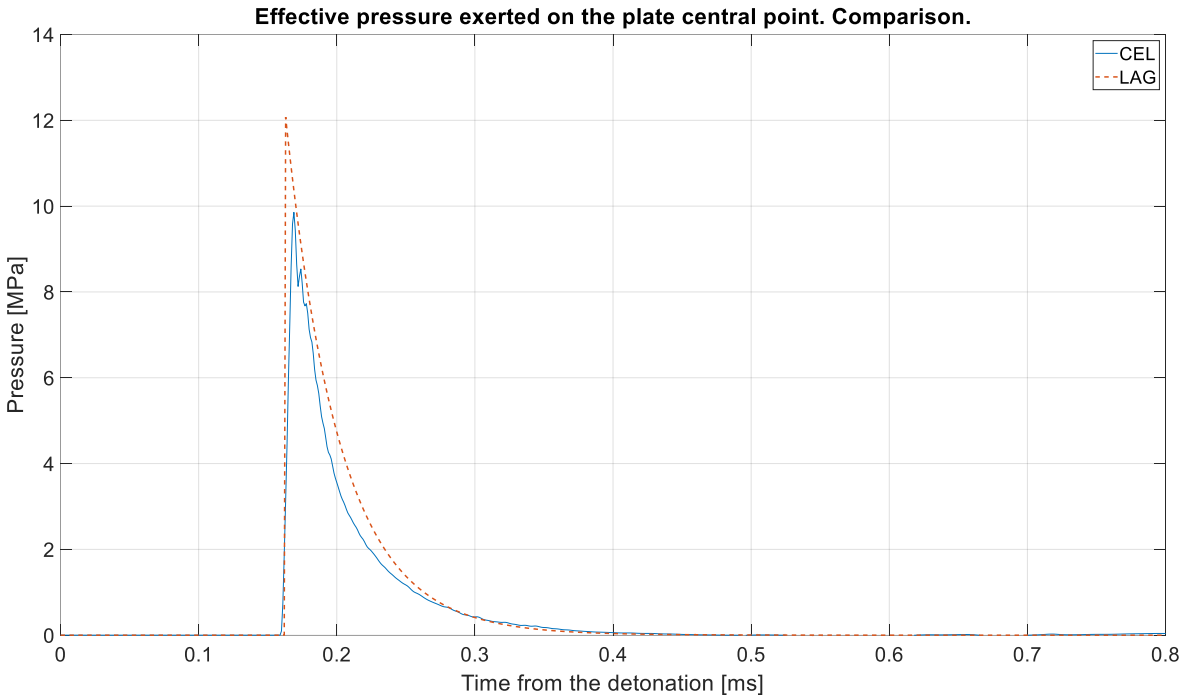

Figure 11. Effective pressure exerted on the plate central point in the analyses presented in Section 3.

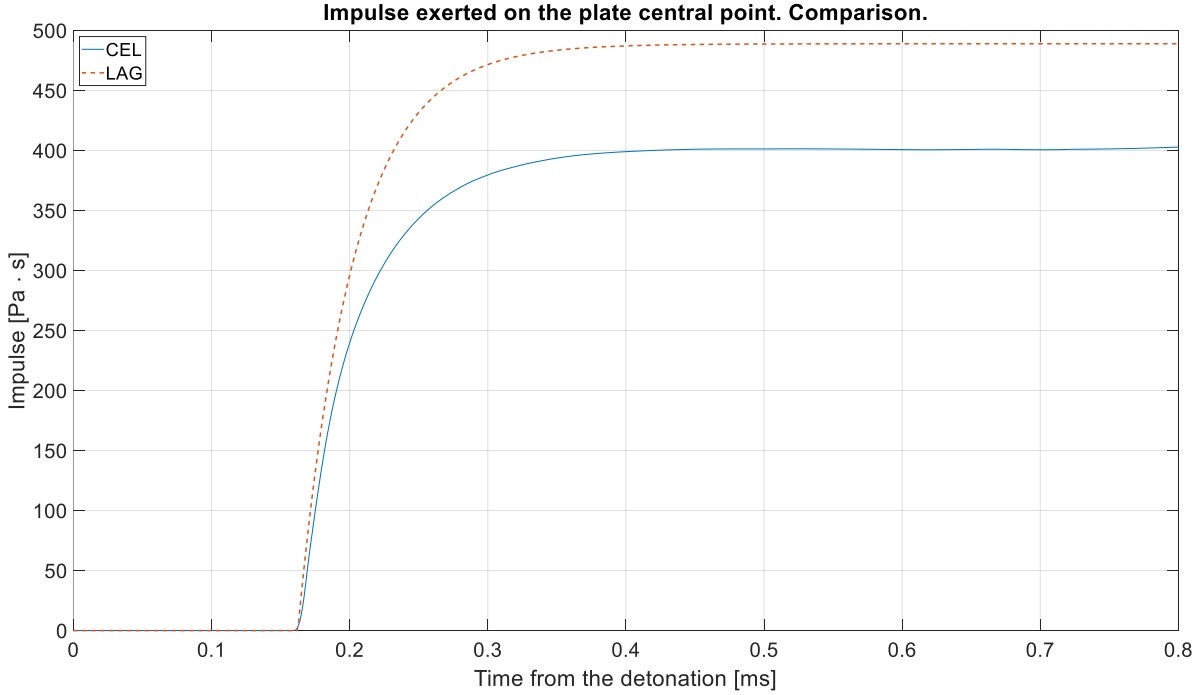

Figure 12. Impulse exerted on the plate central point in the analyses presented in Section 3.

It is worth highlighting that the peak effective pressure and the impulse imparted to the plate were not experimentally measured in the work in [12], hence no further considerations can be given about the corresponding numerical predictions presented herein.

5. Conclusions

In this work, two approaches to simulate blast loaded composite plates have been presented and compared. In particular, the pure Lagrangian approach and a hybrid CEL approach have been described in Section 2 and employed in the case study presented in Section 3. Moreover, the influence of the technique employed to model the plate boundary conditions has been investigated.

As discussed in Section 4, it turns out that explicitly modelling the boundary conditions of the blast loaded plate is paramount to satisfactorily reproduce the experimental observations. Moreover, considering the model characterised by the accurate reproduction of the boundary conditions, the pure Lagrangian approach appears to give slightly more satisfactory results than the predictions provided by the CEL analysis. This may seem unexpected at first sight, but it has been shown that the scenario assessed in the case study presented in Section 3 is a far-field explosion, thus no improvement is expected by employing the CEL approach. The smaller maximum deflection of the plate central point predicted by the CEL analysis is caused by the lower peak effective pressure and impulse imparted to the plate than the values determined by the pure Lagrangian approach. No further considerations have been reported about this dissimilarity, since experimental observations of the pressure loading are not available. More accurate numerical models might be set up to get a deeper insight into the explosive event presented in the case study, but this requires to have (i) experimental data of the pressure time history imparted to the plate, in order to set a more accurate TNT equivalent weight than the one assumed in this work, and (ii) the stress-strain curve of the foam material placed between the composite plate and the steel frame.

References

[1] Yao S, Zhang D and Lu F 2015 Dimensionless numbers for dynamic response analysis of clamped square plates subjected to blast loading *Arch. Appl. Mech. 2015 856* **85** 735–44
[2] Chung Kim Yuen S, Nurick G N, Verster W, Jacob N, Vara A R, Balden V H, Bwalya D, Govender R A and Pittermann M 2008 Deformation of mild steel plates subjected to large-scale explosions *Int. J. Impact Eng.* **35** 684–703
[3] Nurick G N and Martin J B 1989 Deformation of thin plates subjected to impulsive loading—a review Part II: Experimental studies *Int. J. Impact Eng.* **8** 171–86
[4] Nurick G N and Martin J B 1989 Deformation of thin plates subjected to impulsive loading—A review: Part I: Theoretical considerations *Int. J. Impact Eng.* **8** 159–70
[5] Chung Kim Yuen S, Nurick G N, Langdon G S and Iyer Y 2017 Deformation of thin plates subjected to impulsive load: Part III – an update 25 years on *Int. J. Impact Eng.* **107** 1339–51
[6] Langdon G S, Yuen S C K and Nurick G N 2005 Experimental and numerical studies on the response of quadrangular stiffened plates. Part II: localised blast loading *Int. J. Impact Eng.* **31** 85–111
[7] Yuen S C K and Nurick G N 2005 Experimental and numerical studies on the response of quadrangular stiffened plates. Part I: subjected to uniform blast load *Int. J. Impact Eng.* **31** 55–83
[8] Børvik T, Hanssen A G, Langseth M and Olovsson L 2009 Response of structures to planar blast loads – A finite element engineering approach *Comput. Struct.* **87** 507–20
[9] Ziya-Shamami M, Babaei H, Mostofi T M and Khodarahmi H 2020 Structural response of monolithic and multi-layered circular metallic plates under repeated uniformly distributed impulsive loading: An experimental study *Thin-Walled Struct.* **157** 107024
[10] Langdon G S, Cantwell W J, Guan Z W and Nurick G N 2014 The response of polymeric composite structures to air-blast loading: a state-of-the-art *http://dx.doi.org/10.1179/1743280413Y.0000000028* **59** 159–77
[11] Fallah A S, Micallef K, Langdon G S, Lee W C, Curtis P T and Louca L A 2014 Dynamic response of Dyneema® HB26 plates to localised blast loading *Int. J. Impact Eng.* **73** 91–100
[12] Gargano A, Das R and Mouritz A P 2019 Finite element modelling of the explosive blast response of carbon fibre-polymer laminates *Compos. Part B Eng.* **177** 107412

[13] Gunaryo K, Heriana H, Sitompul M R, Kuswoyo A and Hadi B K 2020 Experimentation and numerical modeling on the response of woven glass/epoxy composite plate under blast impact loading *Int. J. Mech. Mater. Eng. 2020 151* **15** 1–9
[14] Turkmen H S 2017 The Dynamic Behavior of Composite Panels Subjected to Air Blast Loading: Experiment and Theory *Explos. Blast Response Compos.* 57–84
[15] Schiffer A and Tagarielli V L 2015 The response of circular composite plates to underwater blast: Experiments and modelling *J. Fluids Struct.* **52** 130–44
[16] Baştürk S, Uyanik H and Kazanci Z 2014 An analytical model for predicting the deflection of laminated basalt composite plates under dynamic loads *Compos. Struct.* **116** 273–85
[17] Mouritz A P 2019 Advances in understanding the response of fibre-based polymer composites to shock waves and explosive blasts *Compos. Part A Appl. Sci. Manuf.* **125** 105502
[18] LeBlanc J and Shukla A 2010 Dynamic response and damage evolution in composite materials subjected to underwater explosive loading: An experimental and computational study *Compos. Struct.* **92** 2421–30
[19] Batra R C and Hassan N M 2008 Blast resistance of unidirectional fiber reinforced composites *Compos. Part B Eng.* **39** 513–36
[20] Lomazzi L, Giglio M and Manes A 2021 Analytical and empirical methods for the characterisation of the permanent transverse displacement of quadrangular metal plates subjected to blast load: comparison of existing methods and development of a novel methodological approach. *Int. J. Impact Eng.* 103890
[21] Aune V, Valsamos G, Casadei F, Langseth M and Børvik T 2021 Fluid-structure interaction effects during the dynamic response of clamped thin steel plates exposed to blast loading *Int. J. Mech. Sci.* **195** 106263
[22] Kingery C N and Bulmash G 1984 *Air Blast Parameters from TNT Spherical Air Burst and Hemispherical Surface Burst* (Aberdeen Proving Ground, Maryland: Ballistic Research Laboratories)
[23] Cranz K J, Eberhard O V. and Becker K E 1926 *Lehrbuch der Ballistik. Ergänzungen zum. Band II* ed Springer (Berlin)
[24] Hopkinson B 1915 *British ordnance board minutes, Report 13565* (London)
[25] Shin J, Whittaker A S and Cormie D 2015 Incident and Normally Reflected Overpressure and Impulse for Detonations of Spherical High Explosives in Free Air *J. Struct. Eng.* **141** 04015057
[26] Randers-Pehrson G, Bannister K A and Qxuaij L C 1997 *Airblast Loading Model for DYNA2D and DYNA3D*
[27] Lomazzi L, Giglio M and Manes A 2021 Analysis of the blast wave – structure interface phenomenon in case of explosive events *IOP Conf. Ser. Mater. Sci. Eng.* **1038** 012083
[28] Lee E L, Hornig H C and Kury J W 1968 *Adiabatic Expansion Of High Explosive Detonation Products* (Livermore, CA (United States))
[29] LIVERMORE SOFTWARE TECHNOLOGY CORPORATION (LSTC) 2018 *LS-DYNA® KEYWORD USER'S MANUAL - VOLUME II Material Models*
[30] Zhang T G, Satapathy S S, Dagro A M and McKee P J 2013 Numerical study of head/helmet interaction due to blast loading *ASME International Mechanical Engineering Congress and Exposition, Proceedings (IMECE)* vol 3 A (American Society of Mechanical Engineers (ASME))
[31] Fitek J and Meyer E 2013 *Design of a Helmet Liner for Improved Low Velocity Impact Protection*
[32] Hashin Z 1980 Failure Criteria for Unidirectional Fiber Composites *J. Appl. Mech.* **47** 329–34
[33] Tiwari A, Dorogin L, Tahir M, Stö K W, Heinrich G, Espallargas N and Persson B N J 2017 Rubber contact mechanics: adhesion, friction and leakage of seals *Soft Matter* **13** 9103
[34] Karger-Kocsis J, Mousa A, Major Z and Békési N 2008 Dry friction and sliding wear of EPDM rubbers against steel as a function of carbon black content *Wear* **264** 359–67
[35] Bogosian D, Yokota M and Rigby S 2016 TNT equivalence of C-4 and PE4: a review of

traditional sources and recent data *undefined*
[36] Touloukian Y S, Liley P E and Saxena S C 1970 *Thermophysical Properties of Matter, Vol. 3: Thermal Conductivity* (NY: IFI/Plenun)
[37] Touloukian Y S, Liley P E and Saxena S C 1970 *Thermophysical Properties of Matter, Vol. 11: Viscosity* (NY: IFI/Plenun)
[38] Shin J, Whittaker A S, Cormie D and Wilkinson W 2014 Numerical modeling of close-in detonations of high explosives *Eng. Struct.* **81** 88–97
[39] Koli S, Chellapandi P, Bhaskara Rao L and Sawant A 2020 Study on JWL equation of state for the numerical simulation of near-field and far-field effects in underwater explosion scenario *Eng. Sci. Technol. an Int. J.* **23** 758–68